Inorganic Chemistry

Article

pubs.acs.org/IC

Luminescent Metallogels of Bis-Cyclometalated Alkynylgold(III) Complexes

Vonika Ka-Man Au, Nianyong Zhu, and Vivian Wing-Wah Yam*

Institute of Molecular Functional Materials [Areas of Excellence Scheme, University Grants Committee (Hong Kong)] and Department of Chemistry, The University of Hong Kong, Pokfulam Road, Hong Kong

Supporting Information

ABSTRACT: A series of luminescent bis-cyclometalated alkynylgold(III) complexes have been synthesized and characterized. Some of the complexes have been demonstrated to exhibit gelation properties driven by $\pi-\pi$ stacking and hydrophobic−hydrophobic interactions. The gelation properties have been investigated in detail through variable-temperature UV−vis absorption and emission studies, and the morphology of the gels has also been characterized by scanning electron microscopy and transmission electron microscopy.

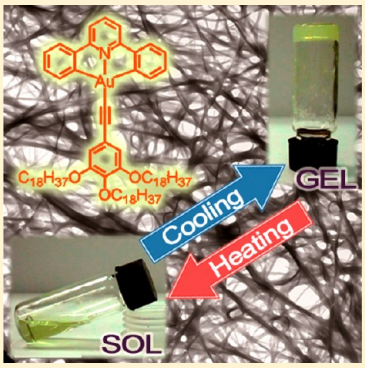

INTRODUCTION

Over the past few decades, a rapid growth of interest in gold chemistry has been observed.[1−11] On the other hand, there has been an enormous increase in attention drawn toward the design and synthesis of novel supramolecular assemblies,[10−19] especially those based on transition metal complex systems.[16−24] Recently, our group has reported the interesting photoluminescence and electroluminescence properties of bis-cyclometalated gold(III) complexes, and it was found that the presence of $\pi-\pi$ stacking interactions among the complex molecules could exert some influence on the emission as well as the electrochemistry of this class of complexes.[25] It is anticipated that such $\pi-\pi$ stacking interactions, together with other intermolecular interactions such as van der Waals' forces, hydrogen bonding, and electrostatic attractions, may function to facilitate the self-assembly of organogold(III) complexes. In fact, the study of luminescent gold(III) complexes is rather underdeveloped and underexplored, which is in contrast to that of the related gold(I) and isoelectronic platinum(II) systems.[11b,c] This probably stems from the presence of low-energy d−d ligand field (LF) states as well as the electrophilicity observed for the gold(III) metal center.[11b,c] In order to enhance the luminescence behavior of gold(III) complexes, one strategy has been through the introduction of strong σ-donating ligands, which has been first demonstrated and reported by the group of Yam on the preparation of stable gold(III) aryl complexes that are found to emit even at room temperature in solution.[26] Later on, this concept has been further extended to bis-cyclometalated gold(III) complexes that contain strongly σ-donating alkynyl and *N*-heterocyclic carbene ligands.[25] Mono-cyclometalated bis-alkynylgold(III) complexes of arylpyridine have also been reported very recently.[27,28] These cyclometalated gold(III) complexes have been observed to exhibit rich luminescence properties at both ambient and low temperatures in various media. Very recently, another class of luminescent gold(III) complexes with electron-rich pentafluorophenyl moieties has been reported. Some of these complexes were found to show room-temperature luminescence that involved participation of the gold(III) metal center.[29]

On the other hand, low-molecular-mass organic gelators (LMOGs) represent a key area in the study of supramolecular assembly because of their spontaneous and controlled self-assembly phenomena.[12−18,30,31] In many cases, LMOGs are formed upon their self-assembly through a combination of non-covalent interactions such as $\pi-\pi$ stacking, hydrogen bonding, hydrophobic−hydrophobic interactions and van der Waals' forces, resulting in the formation of entangled self-assembled fibrillar networks (SAFINs).[13] Owing to these weak intermolecular interactions, the key advantage of using LMOGs as molecular building blocks is their reversibility, which makes them highly tunable and responsive to micro-environmental changes.[32−35] For example, LMOGs of pyrene-containing oligopeptides have been shown to self-assemble to give one-dimensional helical columnar structures that further lead to three-dimensional fibrous networks.[36] Luminescence color switching was observed and was ascribed to the interplay of the $\pi-\pi$ stacking interactions of the pyrene moieties and the intermolecular hydrogen bonding interactions of the oligopeptides.[36]

Stemming from the extensive studies on organogels, there has been an increasing interest in the investigation of

Received: April 12, 2012

   dx.doi.org/10.1021/ic3007519 | *Inorg. Chem.* XXXX, XXX, XXX−XXX

metallogels based on transition metal complex systems such as platinum(II),[37−40] gold(I),[41] copper(I),[42,43] rhenium(I),[44] and iron(II).[45] In particular, luminescent metallogels represent a remarkable class of gelators. The presence of metallophilic interactions and/or non-covalent forces may lead to variation in the gelating abilities and rich photophysical properties. An elegant example based on trinuclear (pyrazolato)gold(I) complexes with long alkyl side chains was reported recently, with reversible RGB-color switching behavior of the gel, where both aurophilic interactions and van der Waals' forces have been shown to be involved.[41] Recent works by us have shown that metallogels based on the platinum(II) and rhenium(I) transition metal systems display rich luminescence behavior.[37,44] In one representative example, luminescence enhancement has been observed at elevated temperatures for a series of alkynylplatinum(II) metallogels bearing pincer ligands derived from 2,6-bis(*N*-alkylbenzimidazol-2′-yl)pyridine.[37c] To the best of our knowledge, corresponding work on gold(III) systems has not been reported. It is believed that, with a judicious selection of the coordinating ligands, luminescent gold(III) complexes with gelation properties could be developed, and the gelation properties could be readily modified through a fine balance and an interplay of the non-covalent interactions between these gelators and the solvent molecules. Herein, we report the functionalization of the bis-cyclometalated gold(III) chromophores with organogelating moieties for the preparation of luminescent gold(III) metallogels.

RESULTS AND DISCUSSION

Synthesis and Characterization. The bis-cyclometalated alkynylgold(III) complexes **1**−**10**, as shown in Chart 1, were synthesized by stirring a mixture of the chlorogold(III) precursor [Au(R-C^N^C)Cl][46] and the respective 3,4,5-(trialkoxyphenyl)acetylene[47] in dichloromethane in the presence of Et_3N and a catalytic amount of CuI at room temperature under a nitrogen atmosphere according to that reported previously by us.[25] All of the complexes are found to be air and thermally stable and soluble in common organic solvents such as dichloromethane and chloroform. The identities of all of the complexes have been confirmed by ^{1}H NMR spectroscopy, fast-atom-bombardment mass spectrometry (FAB-MS), and satisfactory elemental analyses. Their IR spectra exhibited a ν(C≡C) absorption at 2137−2152 cm^{-1}, which is in accordance with the presence of the alkynyl ligand in the terminal σ-coordination mode.

Chart 1

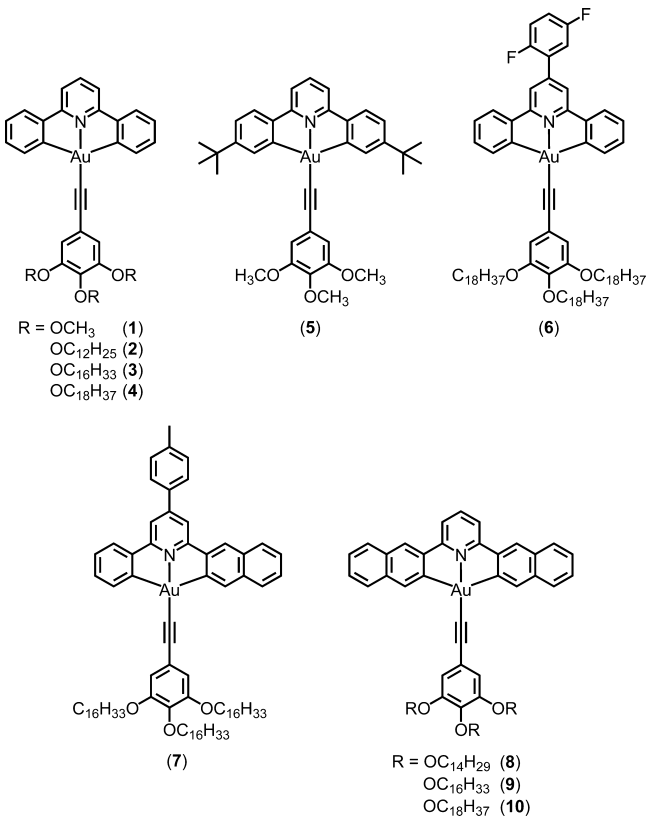

X-ray Crystal Structures. Single crystals of [Au(C^N^C)-(C≡C$C_6H_2(OCH_3)_3$-3,4,5)] (**1**) and [Au(^{t}BuC^N^C^{t}Bu)-(C≡C$C_6H_2(OCH_3)_3$-3,4,5)] (**5**) were obtained by layering of *n*-hexane onto a concentrated dichloromethane solution of the respective complex, and their crystal structures were determined by X-ray crystallography. Crystal structure determination data are summarized in Table 1. The selected bond distances and bond angles are tabulated in Table 2. The perspective views of the crystal structures of **1** and **5** are depicted in Figure 1, and their crystal packing diagrams are shown in Figure 2. The gold(III) metal center coordinates to the tridentate cyclometalating R-C^N^C ligand, with the remaining site occupied by an alkynyl ligand to give a distorted square-planar geometry, characteristic of d^8 metal complexes. The C−Au−N angles of 80.5−81.4° about the gold(III) metal

Table 1. Crystal and Structure Determination Data of Complexes 1 and 5

	[Au(C^N^C)(C≡C$C_6H_2(OCH_3)_3$-3,4,5)]·$^1/_2C_6H_{14}$ (**1**·$^1/_2C_6H_{14}$)	[Au(^{t}BuC^N^C^{t}Bu)(C≡C$C_6H_2(OCH_3)_3$-3,4,5)] (**5**)
empirical formula	$C_{28}H_{22}AuNO_3$·$^1/_2$ C_6H_{14}	$C_{36}H_{38}AuNO_3$
fw	660.52	729.64
temp, K	296(2)	302(2)
wavelength, Å	0.71073	0.71073
cryst syst	monoclinic	monoclinic
space group	$P2_1/n$	$P2_1/c$
a, Å	8.5855(2)	17.1549(7)
b, Å	23.4736(7)	14.2495(6)
c, Å	13.1607(4)	13.0516(6)
α, deg	90	90
β, deg	100.066(2)	100.8060(10)
γ, deg	90	90
volume, cm^3	2611.48(13)	3133.9(2)
Z, Å^3	4	4
density (calcd), g cm^{-3}	1.680	1.546
cryst size, mm^3	0.34 × 0.18 × 0.06	0.49 × 0.18 × 0.05
index ranges	$-10 \le h \le 10$	$-20 \le h \le 19$
	$-27 \le k \le 27$	$-15 \le k \le 16$
	$-15 \le l \le 15$	$-15 \le l \le 15$
reflns collected/ unique	36857/4613	17192/5510
GOF on F^2	1.032	1.069
final *R* indices [$I > 2\sigma(I)$]	R1 = 0.0357, wR2 = 0.0848	R1 = 0.0182, wR2 = 0.0410
largest diff peak and hole, e Å^{-3}	1.324 and −0.899	0.295 and −0.550

dx.doi.org/10.1021/ic3007519 | *Inorg. Chem.* XXXX, XXX, XXX−XXX

Table 2. Selected Bond Lengths (Å) and Angles (deg) for Complexes 1 and 5 with Estimated Standard Deviations (esd's) Given in Parentheses

[Au(C^N^C)(C≡CC$_6$H$_2$(OCH$_3$)$_3$-3,4,5)]·$^1/_2$C$_6$H$_{14}$ (**1**·$^1/_2$C$_6$H$_{14}$)		[Au(^{t}BuC^N^C^{t}Bu)(C≡CC$_6$H$_2$(OCH$_3$)$_3$-3,4,5)] (**5**)	
Bond Lengths (Å)			
Au(1)−C(1)	1.998(7)	Au(1)−C(1)	1.969(3)
Au(1)−C(12)	2.061(8)	Au(1)−C(12)	2.064(3)
Au(1)−C(28)	2.070(7)	Au(1)−C(28)	2.075(3)
Au(1)−N(1)	2.005(5)	Au(1)−N(1)	2.002(2)
C(1)−C(2)	1.142(8)	C(1)−C(2)	1.193(4)
Bond Angles (deg)			
C(12)−Au(1)−C(28)	161.9(3)	C(12)−Au(1)−C(28)	162.10(12)
N(1)−Au(1)−C(1)	179.3(2)	N(1)−Au(1)−C(1)	176.85(10)
Au(1)−C(1)−C(2)	177.2(6)	Au(1)−C(1)−C(2)	174.7(3)
N(1)−Au(1)−C(12)	81.4(3)	N(1)−Au(1)−C(12)	81.04(10)
N(1)−Au(1)−C(28)	80.5(2)	N(1)−Au(1)−C(28)	81.06(11)
C(1)−C(2)−C(3)	177.3(7)	C(1)−C(2)−C(3)	178.5(3)

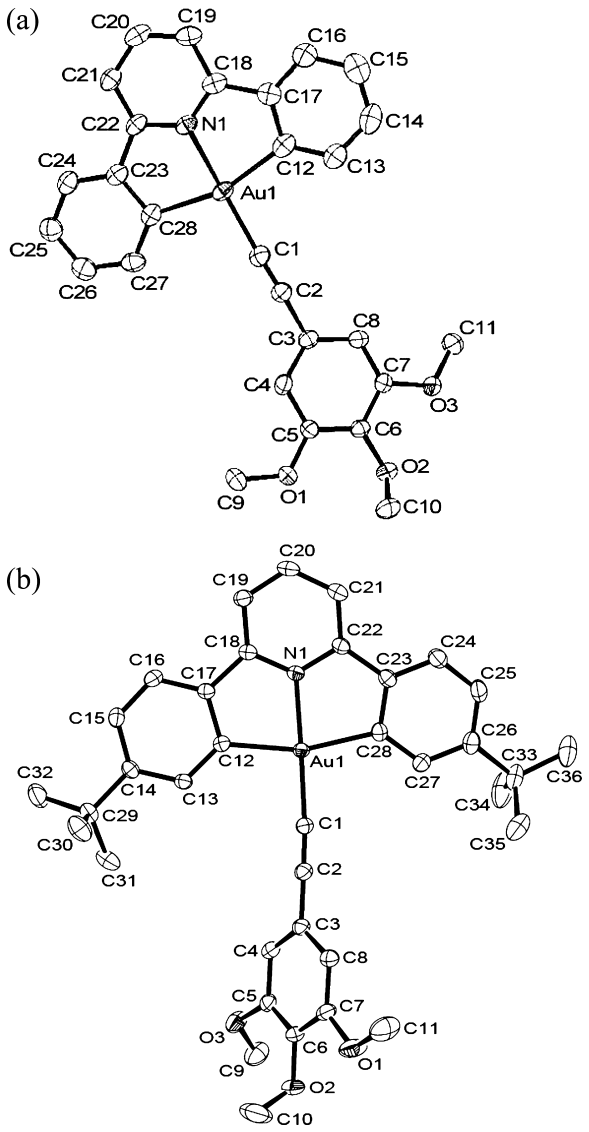

Figure 1. Perspective views of (a) **1** and (b) **5** with atomic numbering schemes. H atoms have been omitted for clarity. Thermal ellipsoids are drawn at the 30% probability level.

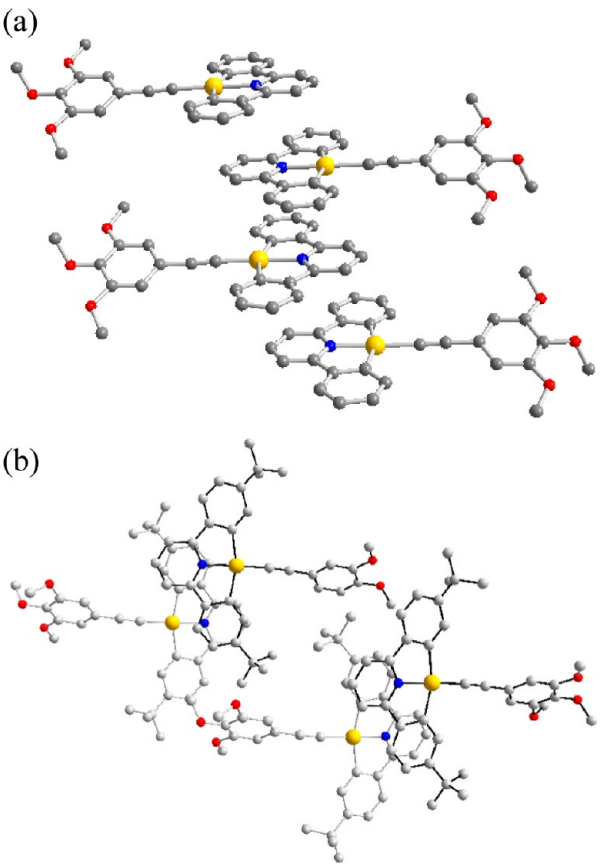

Figure 2. Crystal packing diagrams of (a) **1** and (b) **5**, showing the "dimeric" configuration.

center are found to deviate from the ideal 90° because of the restricted bite angle of the tridentate R-C^N^C ligands. The [Au(R-C^N^C)] motif is essentially coplanar, and the Au−C (2.061−2.075 Å) and Au−N (2.002−2.005 Å) bond distances are similar to those found in other related complexes.[25] The Au−C≡C and C≡C−C angles of 174.7−177.2° and 177.3−178.5° only show a minor deviation from the ideal 180°, establishing a slightly distorted linear arrangement, with the Au−C (1.969−1.998 Å) and C≡C bond distances (1.142−1.193 Å) similar to those found in the related cyclometalated alkynylgold(III) systems.[25,27] Because the shortest Au···Au distances (5.3311 and 5.8769 Å) between adjacent molecules are found to be longer than the sum of the van der Waals radii for two gold(III) centers, no significant Au···Au interactions

dx.doi.org/10.1021/ic3007519 | Inorg. Chem. XXXX, XXX, XXX−XXX

occur in the crystal lattices of the complexes. The molecules are arranged in a head-to-tail fashion in the crystal lattice, with some $\pi-\pi$ stacking interactions of 3.4288−3.5649 Å between the [Au(C^N^C)] moieties.

Electrochemistry. The cyclic voltammograms of **1**−**10** in dichloromethane (0.1 mol dm^{-3} ^{n}Bu$_4$NPF$_6$) generally show one quasi-reversible reduction couple at −1.31 to −1.61 V vs SCE and an irreversible oxidation wave at +1.09 to +1.27 V vs SCE. The electrochemical data are summarized in Table 3.

Table 3. Electrochemical Data for 1−10[a]

complex	oxidation E_{pa}/V vs SCE[b]	reduction $E_{1/2}$/V vs SCE[c] (ΔE_p/mV)
1	+1.16	−1.54 (77)
2	+1.20	−1.54 (79)
3	+1.17	−1.54 (72)
4	+1.18	−1.53 (65)
5	+1.27	−1.61 (71)
6	+1.17	−1.36 (74)
7	+1.12	−1.31 (73)
8	+1.10	−1.56 (77)
9	+1.15	−1.57 (86)
10	+1.09	−1.56 (85)

[a]In a dichloromethane solution with 0.1 M ^{n}Bu$_4$NPF$_6$ as the supporting electrolyte at room temperature; working electrode, glassy carbon; scan rate 100 mV s^{-1}. [b]E_{pa} refers to the anodic peak potential for the irreversible oxidation waves. [c]$E_{1/2} = (E_{pa} + E_{pc})/2$; E_{pa} and E_{pc} are peak anodic and peak cathodic potentials, respectively. $\Delta E_p = |E_{pa} - E_{pc}|$.

Complexes with the same tridentate cyclometalating R-C^N^C ligands are found to show similar potentials for the reduction couples. For example, complexes **1**−**4** bearing the unsubstituted C^N^C ligand all exhibit reduction couples at ca. −1.54 V vs SCE. In view of such an observation, the reduction couples are ascribed to the ligand-centered reduction of the R-C^N^C ligand, and similar assignments have also been made in other related alkynylgold(III) complexes.[25] Complex **5** was observed to show the most negative potential at −1.61 V, which is in agreement with the assignment because the electron-rich *tert*-butyl substituents on the cyclometalating ligand would raise the energy of the π^* orbital and cause the complex to be reduced with more difficulty, leading to a more negative potential. Extended π conjugation upon the introduction of an aryl substituent on the central pyridine ring of the R-C^N^C ligand stabilizes the π^* orbital and leads to a less negative reduction potential for complexes **6** and **7**. The replacement of the phenyl moieties in the R-C^N^C ligand by naphthyl groups does not cause a significant change in the energy of the π^* orbital, as revealed by the similar potentials in **1**−**4** and **8**−**10**, probably supportive of the greater localization of the lowest unoccupied molecular orbital (LUMO) on the pyridine moiety of the R-C^N^C ligand. On the other hand, the irreversible oxidative waves at +1.09 to +1.27 V are assigned to a ligand-centered oxidation of the alkynyl ligand.[25]

UV−Vis Absorption Spectroscopy. The electronic absorption spectra of the complexes show a high-energy absorption band at 306−324 nm and a vibronically structured absorption band at 363−412 nm with extinction coefficients on the order of 10^3-10^4 dm^3 mol^{-1} cm^{-1}. The photophysical data for complexes **1**−**10** are summarized in Table 4 and the representative electronic absorption spectra of complexes **5**−**7** and **10** are depicted in Figure 3. The absorption energy of the low-energy band is found to be quite insensitive to the nature of the alkynyl ligands. The vibrational progressional spacings of the low-energy band at ca. 1200−1400 cm^{-1} are in agreement with the typical skeletal vibrational frequencies of the cyclometalating R-C^N^C ligand. Similar absorption bands could also be observed in the chloro precursor[46] and the related alkynylgold(III) complexes.[25,27] The lower-energy band is assigned as a metal-perturbed intraligand (IL) $\pi-\pi^*$ transition

Table 4. Photophysical Data for 1−10

	absorption[a]	emission		
complex	λ_{max}/nm (ε_{max}/dm^3 mol^{-1} cm^{-1})	medium (T/K)	λ_{max}/nm (τ_0/μs)	Φ_{em}[b]
1	312 (12970), 322 (12115), 363 (4890), 381 (5080), 401 (3595)	CH_2Cl_2 (298)[c]	573 (0.1)	9.9×10^{-3}
		glass (77)[c,d]	470, 503, 536, 576 (207)	
2	312 (18765), 322 (17320), 366 (9025), 382 (9355), 400 (7230)	CH_2Cl_2 (298)[c]	597 (0.2)	8.7×10^{-3}
		glass (77)[c,d]	486, 522, 558 (144)	
3	312 (13785), 324 (11925), 364 (5010), 382 (5430), 400 (4075)	CH_2Cl_2 (298)[c]	602 (6.4)	8.1×10^{-3}
		glass (77)[c,d]	470, 504, 534, 586 (262)	
4	312 (14765), 324 (13295), 366 (5790), 382 (6185), 400 (4250)	CH_2Cl_2 (298)	604 (0.2)	5.2×10^{-3}
		glass (77)[c,d]	471, 502, 537 (180)	
5	314 (18700), 324 (17195), 372 (6305), 390 (6740), 412 (5635)	CH_2Cl_2 (298)	484, 516, 556 (0.1)	4.6×10^{-3}
		glass (77)[c,d]	478, 510, 547 (257)	
6	306 (21090), 370 (5615), 390 (6160), 408 (4600)	CH_2Cl_2 (298)[c]	639 (0.2)	2.8×10^{-3}
		glass (77)[c,d]	511, 538 (102)	
7	310 (18845), 382 (3450), 400 (3380)	CH_2Cl_2 (298)[c]	563, 606, 659 (13)	8.6×10^{-3}
		glass (77)[c,d]	498, 536, 577 (3373)	
8	306 (53765), 346 (22205), 376 (5865), 394 (7015)	CH_2Cl_2 (298)[c]	559, 602, 660sh (64)	6.5×10^{-2}
		glass (77)[c,d]	554, 602, 653 (235)	
9	344 (8340), 378 (3520), 396 (3835)	CH_2Cl_2 (298)[c]	559, 604, 657sh (12)	1.2×10^{-2}
		glass (77)[c,d]	564, 610 (2807)	
10	302 (49670), 376 (21200), 396 (27775)	CH_2Cl_2 (298)[c]	559, 601, 657sh (35)	9.4×10^{-2}
		glass (77)[c,d]	567, 616, 668sh (279)	

[a]In dichloromethane at 298 K. [b]The luminescence quantum yield, measured at room temperature using quinine sulfate as a standard. [c]Vibronic-structured emission band. [d]In EtOH−MeOH−CH_2Cl_2 (40:10:1, v/v).

dx.doi.org/10.1021/ic3007519 | Inorg. Chem. XXXX, XXX, XXX−XXX

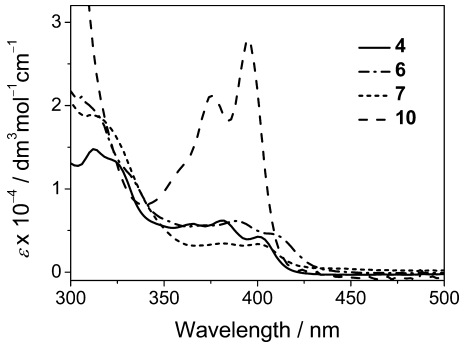

Figure 3. Electronic absorption spectra of complexes **4**, **6**, **7**, and **10** in dichloromethane at 298 K.

of the bis-cyclometalating ligand, with some charge-transfer character from the peripheral phenyl moieties to the central pyridine moiety.

Luminescence Spectroscopy. Upon excitation at $\lambda \geq 330$ nm, the complexes are found to exhibit intense emission in dichloromethane solution at 298 K. Selected solution emission spectra are shown in Figure 4. Considering the emission spectra

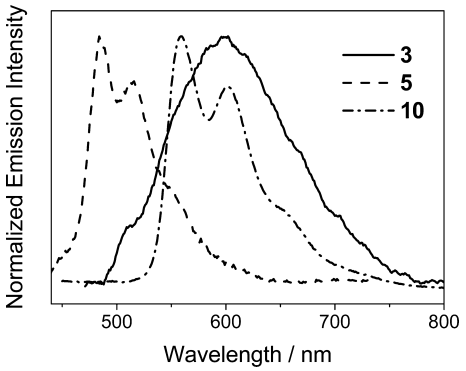

Figure 4. Emission spectra of complexes **3**, **5**, and **10** in dichloromethane at 298 K.

of complexes **1**−**4** and **6**, which all contain an ancillary (trialkoxyphenyl)alkynyl ligand, the complexes are found to exhibit a broad, structureless emission band at 573−639 nm. Complexes **1**−**4**, which contain the same unsubstituted C^N^C ligand, show emission energies that increase from 573 to 604 nm with an increase in the alkoxy chain lengths of the alkynyl ligands. Complex **6**, with an additional difluorophenyl moiety, is found to show an emission band at lower energy at 639 nm. Owing to the electron-rich nature of the (trialkoxyphenyl)-alkynyl ligands, these structureless emission bands are tentatively assigned as originated from an excited state of triplet ligand-to-ligand charge-transfer (^{3}LLCT) [π(C≡CC_6-H_4(OR)$_3$-3,4,5) → π^*(R-C^N^C)] character. However, the presence of (trialkoxyphenyl)alkynyl groups would not always lead to the occurrence of the triplet LLCT emission, as shown in complexes **5** and **7**−**10**, which exhibit a vibronically structured emission band at 484−660 nm. With reference to the emission studies of related bis-cyclometalated gold(III) complexes in the literature,[25] this vibronic-structured emission band can be assigned as originated from an IL ^{3}[$\pi \rightarrow \pi^*$(R-C^N^C)] state, with some charge-transfer character from the aryl moieties to the pyridine moiety of the R-C^N^C ligand. The disappearance of the structureless LLCT emission band could be attributed to the presence of the electron-donating *tert*-butyl and naphthyl groups in the R-C^N^C ligand, which causes the energy levels of the π orbital of the R-C^N^C ligand to be higher-lying than that of the π orbital of the alkynyl ligands. As a result, an emission originating from an IL origin would be preferred to that with a LLCT origin. In the presence of the more conjugated naphthyl moieties in place of phenyl moieties in the cyclometalating R-C^N^C ligand, better delocalization over the cyclometalating ligand would be expected. A pronounced red shift in emission is observed in complex **6** relative to complexes **1**−**4**, as well as in complexes **7**−**10** relative to complex **5**. With increasing conjugation, it is probable that the highest occupied molecular orbital (HOMO) π orbital would be destabilized, while the LUMO π^* orbital would be stabilized, such that the resulting HOMO−LUMO energy gap would be reduced to cause a red shift in emission.

Gelation Studies. The gelation properties of the complexes have been tested in various organic solvents by the "stable to inversion of a test tube" method. The gelation properties of the complexes studied are summarized in Table 5. A range of

Table 5. Summary of Gelation Properties in Various Organic Solvents[a]

complex	DMSO	methanol	hexane	cyclohexane	benzene	toluene
2	I	I	P	P	S	S
3	I	I	P	P	S	S
4	I	I	G_s (4.6)	G_s (4.6)	S	S
6	I	I	G_u	P	S	S
7	I	I	P	P	S	S
8	I	I	P	G_u	S	S
9	I	I	P	G_u	S	S
10	I	I	G_u (20.3)	G_u (25.1)	S	S

[a] G_s = opaque stable gel over 1 week; G_u = unstable gel only stable for a few minutes; P = precipitation; S = soluble; I = insoluble. The values in parentheses are the critical gelation concentrations in mg/mL at 25 °C.

organic solvents, from polar dimethyl sulfoxide (DMSO) to non-polar benzene, have been tested. Complexes **4** and **10** are found to show good gelation behaviors in non-polar organic solvents such as *n*-hexane and cyclohexane and give opaque pale yellow gels. However, the other complexes fail to form any gels in the solvents tested, probably because of an imbalance in the intermolecular interactions, especially hydrophobic−hydrophobic and π−π stacking interactions, between the complex molecules. In particular, the metallogels formed by **4** are highly stable and the critical gelation concentration (cgc) is rather low in hexane and cyclohexane, as shown in Figure 5. On the other hand, the other complexes give only precipitation or insoluble suspensions in these solvents (Table 5).

Electron microscopy was performed on the xerogels (air-dried gels) of the complexes in order to study their morphologies. Xerogels have been employed for the study of a number of organogels[31,36] and metallogels[37−42,44] to investigate their structures by microscopic techniques and have been regarded as a good representation of the real gel structures. Scanning electron microscopy (SEM) and transmission electron microscopy (TEM) images have been recorded for the hexane and cyclohexane xerogels (air-dried gel) formed by complex **4**, as well as the hexane xerogel formed by complex **10**. As in typical organogels and metallogels,[12,14] the gel states of the complexes demonstrated a network of

dx.doi.org/10.1021/ic3007519 | Inorg. Chem. XXXX, XXX, XXX−XXX

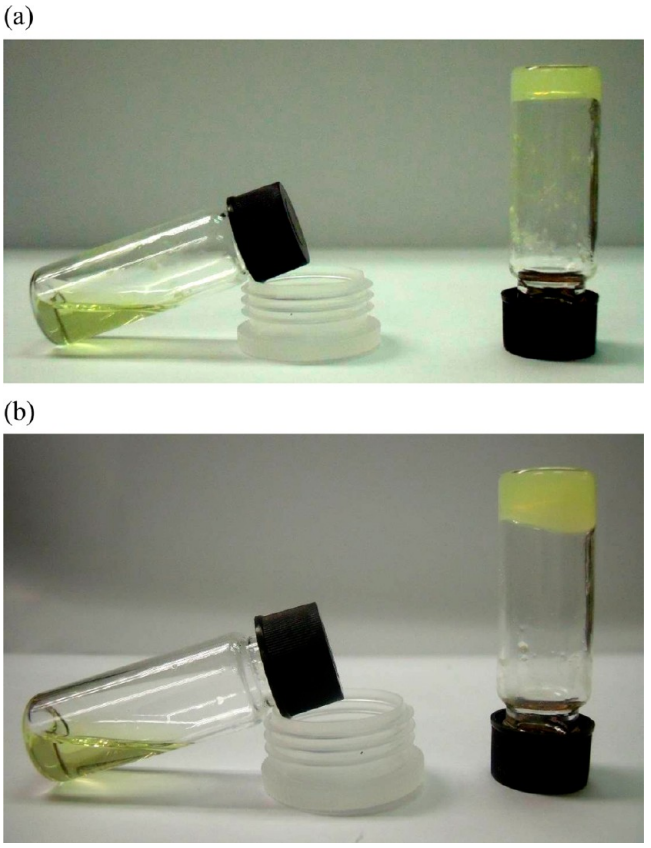

Figure 5. Photographs of (a) the hexane gel and (b) the cyclohexane gel of **4** with the corresponding sol forms at elevated temperature ([Au] = 4.6 mg/mL in both cases).

entangled fibrous structures in a micrometer scale, as shown in the SEM and TEM images in Figures 6 and 7.

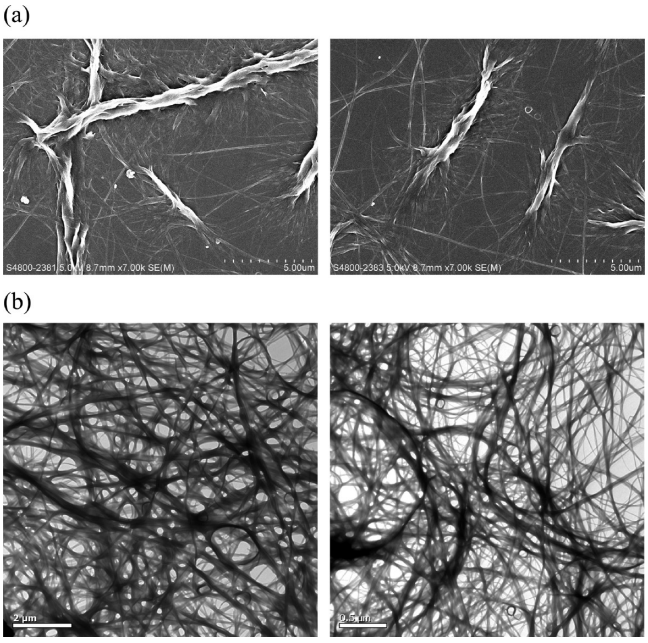

Figure 7. (a) SEM and (b) TEM images of the xerogels prepared from the cyclohexane gel of complex **4**.

In order to clearly observe the gel-to-sol phase transition behavior, temperature-dependent UV−vis absorption studies have been performed for complex **4**. Upon gel-to-sol phase transition at elevated temperatures, complex **4** shows an obvious increase in the color intensity from very pale yellow gel to yellow sol. When the temperature is increased from 10 to 40 °C in hexane, the UV−vis absorption spectra feature a drop in absorbance of the absorption tail at ca. 430 nm and beyond. The vibronically structured absorption bands at 393 and 414 nm gradually merge into a broad absorption band. Beyond 40

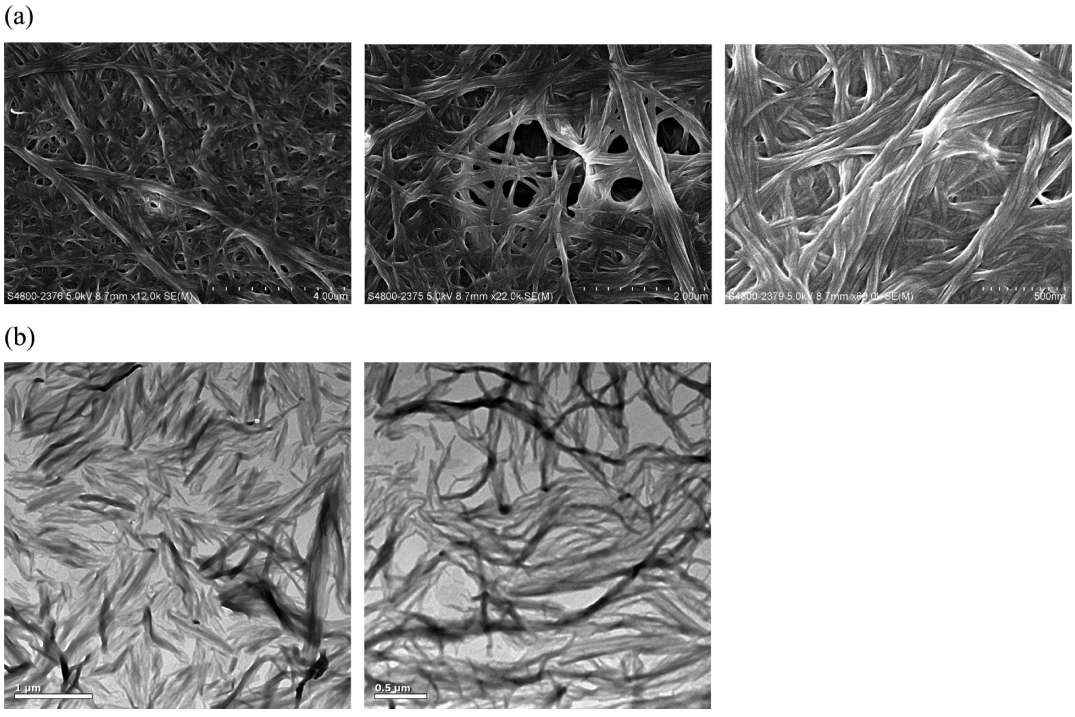

Figure 6. (a) SEM and (b) TEM images of the xerogels prepared from the hexane gel of complex **4**.

dx.doi.org/10.1021/ic3007519 | *Inorg. Chem.* XXXX, XXX, XXX−XXX

°C, a new vibronic band starts to appear at 381 and 401 nm. A further increase in temperature up to 48 °C, which is the sol−gel phase transition temperature (T_{gel}), leads to the complete disappearance of the absorption shoulder. Further heating results only in an increase in the absorbance and very few changes in the shape of the UV−vis absorption spectra. Similar observations have been obtained for the temperature-dependent UV−vis spectroscopic studies of complex **4** in cyclohexane. Complex **4** forms a pale yellow gel in cyclohexane and would give a more intensely colored yellow sol upon a gel-to-sol phase transition at higher temperatures. Initially, in the hexane gel at 10 °C, complex **4** features vibronically structured absorption bands at 395 and 415 nm and an absorption shoulder at 430 nm. When the temperature is increased, the UV−vis absorption spectra also display a drop in the intensity of the absorption tail beyond 430 nm. The vibronically structured band gradually disappears and new vibronic bands are developed at 385 and 400 nm when the temperature is above 23 °C. At the phase transition temperature of 35 °C, the absorption shoulder completely disappears, and the absorbance of the new vibronically structured band is found to increase with temperature. The UV−vis absorption spectral traces at various temperatures in hexane and cyclohexane are depicted in Figures 8 and S1 in the Supporting Information (SI), respectively. With

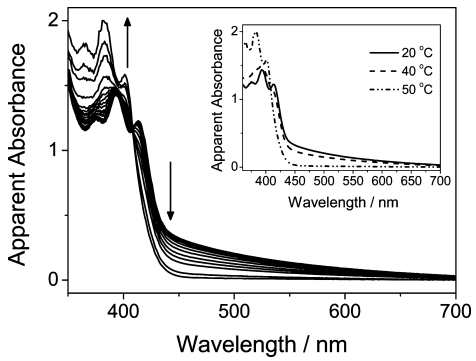

Figure 8. UV−Vis absorption spectral traces of the sol−gel phase transition of complex **4** in hexane upon an increase in the temperature from 10 to 50 °C. Inset: spectral traces at 20, 40, and 50 °C.

reference to the electronic absorption studies of these complexes, the vibronically structured bands are assigned as the IL transition of the cyclometalating C^N^C ligand. The exhibition of an isosbestic point at 408−410 nm suggests a clean conversion from the supramolecular assemblies to the monomeric species upon a gel-to-sol transition at elevated temperature. On the other hand, complex **10** shows a less dramatic color change upon sol−gel phase transition in cyclohexane or hexane, and the gels are less stable than those of complex **4**. Upon an increase in the temperature, the yellow gel of complex **10** would gradually become a sol, which is also yellow in color.

The corresponding variable-temperature emission properties of the hexane and cyclohexane gels have also been investigated for complex **4**. The complex shows similar emission bands in both solvents. Upon excitation at the isosbestic point at ca. 410 nm at 10 °C, an emission band is observed at 570−620 nm, which is assigned as originated from the ^{3}LLCT [π(C≡C $C_6H_4(OR)_3$-3,4,5) → π^*(C^N^C)] excited state. When the temperature is raised, the intensity of the emission band is found to drop. In cyclohexane, the complex shows additional vibronic-structured emission bands at 496 and 526 nm upon transition to the sol form when the temperature is increased to 30 °C, which is assignable to a ^{3}IL [$\pi \rightarrow \pi^*$(C^N^C)] excited state. The observation of both the IL and LLCT bands suggests that the two states are rather close-lying in energy. At elevated temperatures, both bands show a drop in the emission intensity. This could be explained by the fact that, in the gel state, the rigidity of the media would increase and result in a reduction of molecular vibrations and motions, such that the non-radiative deactivation pathways could be retarded. However, at higher temperatures, the non-radiative decay would become more facile. The emission spectral changes of complex **4** at various temperatures are depicted in Figures 9 and S2 in the SI.

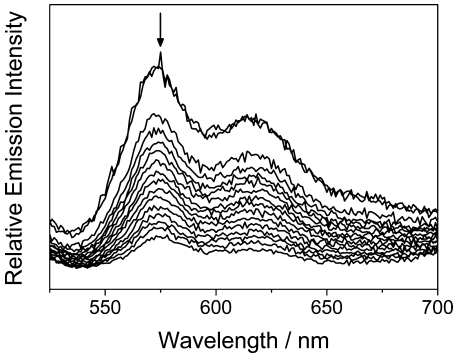

Figure 9. Corrected emission spectra of the hexane gel of complex **4** upon an increase in the temperature from 10 to 40 °C.

CONCLUSION

A bis-cyclometalated alkynylgold(III) system has been found to form metallogels with detectable absorption and emission changes during the sol−gel transition, which can serve as a probe for micro-environmental changes. Microscopic analyses of the xerogels display a network of fibrous structures. With a judicious choice of coordinating ligands, the interplay of non-covalent interactions such as $\pi-\pi$ stacking and hydrophobic−hydrophobic interactions can be readily adjusted for a rational design of metallogels based on the gold(III) system.

EXPERIMENTAL SECTION

Materials and Reagents. Potassium tetrachloroaurate(III) was purchased from ChemPur. The chlorogold(III) precursor complexes, [Au(R-C^N^C)Cl], were prepared according to a literature procedure,[46] using the commercially available 2,6-diphenylpyridine or its derivatives synthesized by the Kröhnke procedure of pyridine synthesis.[48] 3,4,5-Tris(alkoxyphenyl)acetylenes were prepared according to a reported procedure.[47] Copper(I) iodide was obtained from Lancaster and triethylamine from Acros. All solvents were purified and distilled using standard procedures before use. All other reagents were of analytical grade and were used as received.

Physical Measurements and Instrumentation. UV−Vis spectra were obtained on a Hewlett-Packard 8452A diode-array spectrophotometer. ^{1}H NMR spectra were recorded on a Bruker DPX-300 (300 MHz) or Bruker DPX-400 (400 MHz) Fourier transform NMR spectrometer with chemical shifts recorded relative to tetramethylsilane (Me_4Si). Positive FAB-MS spectra were recorded on a Finnigan MAT95 mass spectrometer. Elemental analyses for the metal complexes were performed on the Carlo Erba 1106 elemental analyzer at the Institute of Chemistry, Chinese Academy of Sciences, in Beijing. Steady-state excitation and emission spectra were recorded on a Spex Fluorolog-2 model F111 fluorescence spectrofluorometer equipped with a Hamamatsu R-928 photomultiplier tube. Photo-

dx.doi.org/10.1021/ic3007519 | Inorg. Chem. XXXX, XXX, XXX−XXX

physical measurements in low-temperature glass were carried out with the sample solution loaded in a quartz tube inside a quartz-walled Dewar flask. Liquid nitrogen was placed in the Dewar flask for low-temperature (77 K) photophysical measurements. Excited-state lifetimes of solution samples were measured using a conventional laser system. The excitation source used was the 355-nm output (third harmonic, 8 ns) of a Spectra-Physics Quanta-Ray Q-switched GCR-150 pulsed Nd:YAG laser (10 Hz). Luminescence quantum yields were measured by the optical dilute method reported by Demas and Crosby.[49] A degassed aqueous solution of quinine sulfate in 1.0 N sulfuric acid (Φ = 0.546, excitation wavelength at 365 nm) was used as the reference and corrected for the refractive index of the solution.[49b] All solution samples for photophysical studies were freshly prepared under a high vacuum in a 10-cm^3 round-bottomed flask equipped with a side-arm 1-cm fluorescence cuvette and sealed from the atmosphere by a Rotaflo HP6/6 quick-release Teflon stopper. Solutions were rigorously degassed on a high-vacuum line in a two-compartment cell with no less than four successive freeze–pump–thaw cycles. Cyclic voltammetric measurements were performed by using a CH Instruments, Inc., model CHI 600A electrochemical analyzer. The electrolytic cell used was a conventional two-compartment cell. Electrochemical measurements were performed in dichloromethane solutions with 0.1 M ^{n}Bu$_4$NPF$_6$ as the supporting electrolyte at room temperature. The reference electrode was a Ag/AgNO$_3$ (0.1 M in acetonitrile) electrode, and the working electrode was a glassy carbon electrode (CH Instruments, Inc.) with a platinum wire as the counter electrode. The working electrode surface was first polished with a 1-μm alumina slurry (Linde), followed by a 0.3-μm alumina slurry, on a microcloth (Buehler Co.). The ferrocenium/ferrocene couple ($FeCp_2^{+/0}$) was used as the internal reference.[50] All solutions for electrochemical studies were deaerated with prepurified argon gas just before measurements.

Gelation Studies. A gelation test was carried out by suspending a weighed sample of the gold(III) metallogelator in a measured volume of a particular organic solvent inside a screw-capped sample vial. The suspension was heated until all of the solids were dissolved. The sample vial was cooled in air to room temperature and then left to stand for a period of time. The gelation properties were evaluated by the "stable-to-inverion of a test tube" method. The temperature-dependent electronic absorption spectra and variable-temperature steady-state emission and excitation spectra were obtained using a Varian Cary 50 UV–vis spectrophotometer and a Spex Fluorolog-3 model FL3-211 spectrofluorometer, respectively, with a Varian Cary single-cell Peltier thermostat to control the working temperature. A quartz cuvette with a 2-mm path length has been used for the measurements. SEM experiments were performed either on a Leo1530 field-emission-gun scanning electron microscope or a Hitachi S-3400N variable-pressure scanning electron microscope operating at 4.0–8.0 or 12 kV, respectively. TEM experiments were performed on a Philips Tecnai G2 20 S-TWIN transmission electron microscope with an accelerating voltage of 200 kV. The TEM images were obtained by Gatan MultiScan model 794. Both types of experiments were conducted at the Electron Microscope Unit of the University of Hong Kong. The SEM and TEM samples were prepared by dropping dilute gels onto a silicon wafer. Slow evaporation of the solvents in air for 10 min led to xerogels. All of the samples for SEM experiments were sputter-coated with a gold thin film.

Crystal Structure Determination. Single crystals of **1** and **5** suitable for X-ray diffraction studies were grown by layering of *n*-hexane onto a concentrated dichloromethane solution of the complex. The X-ray diffraction data were collected on a Bruker Smart CCD 1000, using graphite-monochromatized Mo-Kα radiation (λ = 0.71073 Å). The structure was solved by direct methods, employing the *SHELXS-97* program.[51] Full-matrix least-squares refinement on F^2 was used in the structure refinement. The positions of H atoms were calculated based on the riding mode with thermal parameters equal to 1.2 times those of the associated C atoms and participated in the calculation of the final *R* indices. In the final stage of least-squares refinement, all non-H atoms were refined anisotropically.

Synthesis. *General Procedure for Syntheses of Alkynylgold(III) Complexes.* The alkynylgold(III) complexes were synthesized according to a reported procedure, as summarized below.[25] A mixture of the gold(III) precursor complex, [Au(R-C^N^C)Cl] (0.50 mmol), was suspended in dichloromethane (35 mL) in the presence of a catalytic amount of copper(I) iodide (10 mg, 0.05 mmol). The appropriate acetylene (0.75 mmol) and triethylamine (2 mL) were then added. The resulting mixture was stirred at room temperature for 3 h, after which the mixture was evaporated to dryness. The solid residue was purified by column chromatography on silica gel using dichloromethane as the eluent. Subsequent recrystallization from the slow diffusion of diethyl ether or *n*-pentane vapor into the concentrated dichloromethane solution yielded the respective complex as yellow solids.

*[Au(C^N^C)(C≡CC$_6$H$_2$(OCH$_3$)$_3$-3,4,5)] (**1**; HC^N^CH = 2,6-Diphenylpyridine).* **1** was synthesized from [Au(C^N^C)Cl] (231 mg, 0.50 mmol) and 3,4,5-(trimethoxyphenyl)acetylene (144 mg, 0.75 mmol) according to the general procedure. The target complex **1** was obtained as yellow crystals. Crystals of diffraction quality were obtained from the layering of hexane onto a concentrated dichloromethane solution of the complex. Yield: 161 mg (52%). ^{1}H NMR (400 MHz, $CDCl_3$, 298 K): δ 3.88 (s, 3H, −OCH$_3$), 3.91 (s, 6H, −OCH$_3$), 6.86 (s, 2H, −C≡CC$_6$H$_2$−), 7.25 (t, 2H, *J* = 7.3 Hz, phenyl of C^N^C), 7.40 (t, 2H, *J* = 7.3 Hz, phenyl of C^N^C), 7.53 (d, 2H, *J* = 8.0 Hz, pyridine of C^N^C), 7.59 (d, 2H, *J* = 7.3 Hz, phenyl of C^N^C), 7.92 (t, 1H, *J* = 8.0 Hz, pyridine of C^N^C), 8.08 (d, 2H, *J* = 7.3 Hz, phenyl of C^N^C). Positive FAB-MS: *m*/*z* 617 ([M]$^+$). IR (KBr): 2137 cm^{-1} [ν(C≡C)]. Elem anal. Calcd for $C_{28}H_{22}AuNO_3$ (found): C, 54.47 (54.43); H, 3.59 (3.96); N, 2.27 (2.26).

*[Au(C^N^C)(C≡CC$_6$H$_2$(OC$_{12}$H$_{25}$)$_3$-3,4,5)] (**2**).* **2** was synthesized from [Au(C^N^C)Cl] (231 mg, 0.50 mmol) and 3,4,5-(tridodecoxyphenyl)acetylene (491 mg, 0.75 mmol) according to the general procedure. The target complex **2** was obtained as yellow solids. Yield: 270 mg (50%). ^{1}H NMR (400 MHz, CD_2Cl_2, 298 K): δ 0.86 (m, 9H, −CH$_3$), 1.27 (m, 48H, −CH$_2$−), 1.48 (m, 6H, −CH$_2$−), 1.82 (m, 6H, −CH$_2$−), 4.01 (m, 6H, −OCH$_2$−), 6.77 (s, 2H, −C≡C C$_6$H$_2$−), 7.24 (dt, 2H, *J* = 1.1 and 7.3 Hz, phenyl of C^N^C), 7.36 (dt, 2H, *J* = 1.1 and 7.3 Hz, phenyl of C^N^C), 7.50 (d, 2H, *J* = 8.0 Hz, pyridine of C^N^C), 7.59 (d, 2H, *J* = 7.3 Hz, phenyl of C^N^C), 7.88 (t, 1H, *J* = 8.0 Hz, pyridine of C^N^C), 7.99 (d, 2H, *J* = 7.3 Hz, phenyl of C^N^C). Positive FAB-MS: *m*/*z* 1080 ([M]$^+$). IR (KBr): 2137 cm^{-1} [ν(C≡C)]. Elem anal. Calcd for $C_{61}H_{88}AuNO_3 \cdot {}^1/_2H_2O$ (found): C, 67.26 (67.29); H, 8.24 (7.91); N, 1.29 (1.25).

*[Au(C^N^C)(C≡CC$_6$H$_2$(OC$_{16}$H$_{33}$)$_3$-3,4,5)] (**3**).* **3** was synthesized from [Au(C^N^C)Cl] (231 mg, 0.50 mmol) and 3,4,5-(trihexadecoxyphenyl)acetylene (618 mg, 0.75 mmol) according to the general procedure. The target complex **3** was obtained as yellow solids. Yield: 499 mg (80%). ^{1}H NMR (300 MHz, $CDCl_3$, 298 K): δ 0.91 (m, 18H, −CH$_3$ and −CH$_2$−), 1.26 (m, 60H, −CH$_2$−), 1.48 (m, 9H, −CH$_2$−), 1.80 (m, 6H, −CH$_2$−), 3.99 (m, 6H, −OCH$_2$−), 6.83 (s, 2H, −C≡CC$_6$H$_2$−), 7.28 (d, 2H, *J* = 7.3 Hz, phenyl of C^N^C), 7.40 (t, 2H, *J* = 7.3 Hz, phenyl of C^N^C), 7.50 (d, 2H, *J* = 8.1 Hz, pyridine of C^N^C), 7.57 (d, 2H, *J* = 7.3 Hz, phenyl of C^N^C), 7.88 (t, 1H, *J* = 8.1 Hz, pyridine of C^N^C), 8.10 (d, 2H, *J* = 7.3 Hz, phenyl of C^N^C). Positive FAB-MS: *m*/*z* 1249 ([M]$^+$). IR (KBr): 2137 cm^{-1} [ν(C≡C)]. Elem anal. Calcd for $C_{73}H_{112}AuNO_3 \cdot H_2O$ (found): C, 69.22 (69.22); H, 9.07 (8.99); N, 1.11 (1.08).

*[Au(C^N^C)(C≡CC$_6$H$_2$(OC$_{18}$H$_{37}$)$_3$-3,4,5)] (**4**).* **4** was synthesized from [Au(C^N^C)Cl] (231 mg, 0.50 mmol) and 3,4,5-(trioctadecoxyphenyl)acetylene (681 mg, 0.75 mmol) according to the general procedure. The target complex **4** was obtained as pale yellow solids. Yield: 373 mg (56%). ^{1}H NMR (300 MHz, CD_2Cl_2, 298 K): δ 0.80 (m, 9H, −CH$_3$), 1.18 (m, 66H, −CH$_2$−), 1.45 (m, 24H, −CH$_2$−), 1.72 (m, 6H, −CH$_2$−), 3.91 (m, 6H, −OCH$_2$−), 6.71 (s, 2H, −C≡CC$_6$H$_2$−), 7.23 (dt, 2H, *J* = 1.2 and 7.9 Hz, phenyl of C^N^C), 7.33 (dt, 2H, *J* = 1.2 and 7.9 Hz, phenyl of C^N^C), 7.43 (d, 2H, *J* = 7.9 Hz, phenyl of C^N^C), 7.48 (d, 2H, *J* = 7.9 Hz, pyridine of C^N^C), 7.55 (dd, 2H, *J* = 1.2 and 7.9 Hz, phenyl of C^N^C), 7.85 (t, 1H, *J* = 7.9 Hz, pyridine of C^N^C), 7.95 (dd, 2H, *J* = 1.2 and 7.9 Hz, phenyl of C^N^C). Positive FAB-MS: *m*/*z* 1332 ([M]$^+$). IR (KBr):

dx.doi.org/10.1021/ic3007519 | *Inorg. Chem.* XXXX, XXX, XXX–XXX

2145 cm^{-1} [ν(C≡C)]. Elem anal. Calcd for $C_{79}H_{124}AuNO_3 \cdot {}^1/_2CH_2Cl_2$ (found): C, 69.43 (69.82); H, 9.16 (9.16); N, 1.02 (1.25).

*[Au(^{t}BuC^N^C^{t}Bu)(C≡CC_6H_2(OCH$_3$)$_3$-3,4,5)] [**5**; H^{t}BuC^N^C^{t}BuH = 2,6-Bis(4-tert-butylphenyl)pyridine].* **5** was synthesized from [Au(^{t}BuC^N^C^{t}Bu)Cl] (287 mg, 0.50 mmol) and 3,4,5-(trimethoxyphenyl)acetylene (144 mg, 0.75 mmol) according to the general procedure. The target complex **5** was obtained as yellow crystals. Crystals of diffraction quality were obtained from layering of hexane onto a concentrated dichloromethane solution of the complex. Yield: 164 mg (45%). ^{1}H NMR (400 MHz, $CDCl_3$, 298 K): δ 1.39 (s, 18H, ^{t}Bu), 3.89 (s, 3H, −OCH$_3$), 3.90 (s, 6H, −OCH$_3$), 6.88 (s, 2H, −C≡CC_6H_2−), 7.29 (dd, 2H, J = 2.0 and 8.0 Hz, phenyl of C^N^C), 7.41 (d, 2H, J = 8.0 Hz, pyridine of C^N^C), 7.51 (d, 2H, J = 8.0 Hz, phenyl of C^N^C), 7.82 (t, 1H, J = 8.0 Hz, pyridine of C^N^C), 8.22 (d, 2H, J = 2.0 Hz, phenyl of C^N^C). Positive FAB-MS: m/z 730 ([M]$^+$). IR (KBr): 2137 cm^{-1} [ν(C≡C)]. Elem anal. Calcd for $C_{36}H_{38}AuNO_3$ (found): C, 59.26 (59.11); H, 5.25 (5.20); N, 1.92 (2.15).

*[Au{C^N(2,5-F$_2$C$_6$H$_3$)^C}(C≡CC_6H_2(OC$_{18}$H$_{37}$)$_3$-3,4,5)] [**6**; HC^N-(2,5-F$_2$C$_6$H$_3$)^CH = 2,6-Diphenyl-4-(2,5-difluorophenyl)pyridine].* **6** was synthesized from [Au{C^N(2,5-F$_2$C$_6$H$_3$)^C}Cl] (287 mg, 0.50 mmol) and 3,4,5-(trioctadecoxyphenyl)acetylene (681 mg, 0.75 mmol) according to the general procedure. The target complex **6** was obtained as yellow solids. Yield: 520 mg (72%). ^{1}H NMR (300 MHz, $CDCl_3$, 298 K): δ 0.88 (m, 9H, −CH$_3$), 1.25 (m, 84H, −CH$_2$−), 1.48 (m, 6H, −CH$_2$−), 1.82 (m, 6H, −CH$_2$−), 3.98 (m, 6H, −OCH$_2$−), 6.83 (s, 2H, −C≡CC_6H_2−), 7.28−7.33 (m, 5H, −$C_6H_3F_2$-2,5 and phenyl of C^N^C), 7.43 (t, 2H, J = 7.2 Hz, phenyl of C^N^C), 7.63 (m, 4H, −$C_6H_3F_2$-2,5 and pyridine of C^N^C), 8.13 (d, 2H, J = 7.2 Hz, phenyl of C^N^C). Positive FAB-MS: m/z 1445 ([M]$^+$). IR (KBr): 2137 cm^{-1} [ν(C≡C)]. Elem anal. Calcd for $C_{85}H_{126}AuF_2NO_3 \cdot 3H_2O$ (found): C, 68.11 (68.15); H, 8.88 (8.68); N, 0.93 (0.96).

*[Au{C^N(4-MeC$_6$H$_4$)^C$_{Np}$}(C≡CC_6H_2(OC$_{16}$H$_{33}$)$_3$-3,4,5)] (**7**; HC^N-(4-MeC$_6$H$_4$)^C$_{Np}$H = 4-(4-Methylphenyl)-2-(2-naphthyl)-6-phenylpyridine).* **7** was synthesized from [Au{C^N(4-MeC$_6$H$_4$)^C$_{Np}$}Cl] (301 mg, 0.50 mmol) and 3,4,5-(trihexadecoxyphenyl)acetylene (618 mg, 0.75 mmol) according to the general procedure. The target complex **7** was obtained as yellow crystals. Yield: 465 mg (67%). ^{1}H NMR (400 MHz, $CDCl_3$, 298 K): δ 0.88 (m, 24H, −CH$_3$ and −CH$_2$−), 1.26 (m, 54H, −CH$_2$−), 1.43 (m, 9H, −CH$_2$−), 1.78 (m, 9H, −CH$_2$−), 2.47 (s, 3H, −CH$_3$), 3.91 (m, 6H, −OCH$_2$−), 6.67 (s, 2H, −C≡CC_6H_2−), 7.37 (d, 2H, J = 8.1 Hz, −C_6H_4−), 7.41 (d, 1H, J = 8.1 Hz, −C_6H_4−), 7.57 (m, 2H, phenyl of C^N^C), 7.69 (m, 4H, naphthyl and phenyl of C^N^C), 7.82 (m, 1H, naphthyl of C^N^C), 7.93 (m, 2H, pyridine of C^N^C), 7.99 (m, 1H, naphthyl of C^N^C), 8.08 (m, 1H, naphthyl of C^N^C), 8.16 (m, 1H, naphthyl of C^N^C). Positive FAB-MS: m/z 1389 ([M]$^+$). IR (KBr): 2152 cm^{-1} [ν(C≡C)]. Elem anal. Calcd for $C_{84}H_{120}AuNO_3 \cdot 5H_2O$ (found): C, 68.22 (68.24); H, 8.86 (9.04); N, 0.95 (0.88).

*[Au(C$_{Np}$^N^C$_{Np}$)(C≡CC_6H_2(OC$_{14}$H$_{28}$)$_3$-3,4,5)] (**8**; HC$_{Np}$^N^C$_{Np}$H = 2,6-Di-2-naphthylpyridine).* **8** was synthesized from [Au(C^$_{Np}$N^C$_{Np}$)Cl] (281 mg, 0.50 mmol) and 3,4,5-(tritetradecoxyphenyl)acetylene (554 mg, 0.75 mmol) according to the general procedure. The target complex **8** was obtained as pale yellow solids. Yield: 202 mg (32%). ^{1}H NMR (300 MHz, $CDCl_3$, 298 K): δ 0.88 (m, 6H, −CH$_3$), 1.26 (m, 69H, −CH$_3$ and −CH$_2$−), 1.82 (m, 6H, −CH$_2$−), 3.97 (m, 6H, −OCH$_2$−), 6.71 (s, 2H, −C≡CC_6H_2−), 7.54 (m, 4H, naphthyl of C^N^C), 7.91 (m, 4H, naphthyl of C^N^C), 8.00 (m, 3H, naphthyl and pyridine of C^N^C), 8.38 (d, 2H, J = 8.6 Hz, naphthyl of C^N^C), 8.65 (s, 2H, pyridine of C^N^C). Positive FAB-MS: m/z 1265 ([M]$^+$). IR (KBr): 2137 cm^{-1} [ν(C≡C)]. Elem anal. Calcd for $C_{75}H_{101}AuNO_3 \cdot 3C_5H_{12}$ (found): C,73.14 (73.34); H, 9.34 (9.10); N, 0.95 (1.35).

*[Au(C$_{Np}$^N^C$_{Np}$)(C≡CC_6H_2(OC$_{16}$H$_{33}$)$_3$-3,4,5)] (**9**).* **9** was synthesized from [Au(C$_{Np}$^N^C$_{Np}$)Cl] (281 mg, 0.50 mmol) and 3,4,5-(trihexadecoxyphenyl)acetylene (618 mg, 0.75 mmol) according to the general procedure. The target complex **9** was obtained as pale yellow solids. Yield: 513 mg (76%). ^{1}H NMR (400 MHz, $CDCl_3$, 298 K): δ 0.88 (m, 6H, −CH$_3$), 1.26 (m, 75H, −CH$_3$ and −CH$_2$−), 1.45 (m, 6H, −CH$_2$−), 1.80 (m, 6H, −CH$_2$−), 3.91 (m, 6H, −OCH$_2$−), 6.66 (s, 2H, −C≡CC_6H_2−), 7.53 (m, 4H, naphthyl of C^N^C), 7.89 (m, 5H, naphthyl and pyridine of C^N^C), 8.00 (m, 4H, naphthyl and pyridine of C^N^C), 8.36 (d, 2H, J = 8.5 Hz, naphthyl of C^N^C). Positive FAB-MS: m/z 1349 ([M]$^+$). IR (KBr): 2145 cm^{-1} [ν(C≡C)]. Elem anal. Calcd for $C_{81}H_{116}AuNO_3$ (found): C, 72.13 (72.19); H, 8.67 (8.67); N, 1.04 (1.34).

*[Au(C$_{Np}$^N^C$_{Np}$)(C≡CC_6H_2(OC$_{18}$H$_{37}$)$_3$-3,4,5)] (**10**).* **10** was synthesized from [Au(C$_{Np}$^N^C$_{Np}$)Cl] (281 mg, 0.50 mmol) and 3,4,5-(trioctadecoxyphenyl)acetylene (681 mg, 0.75 mmol) according to the general procedure. The target complex **10** was obtained as pale yellow solids. Yield: 107 mg (15%). ^{1}H NMR (300 MHz, $CDCl_3$, 298 K): δ 0.86 (m, 12H, −CH$_3$ and −CH$_2$−), 1.25 (m, 84H, −CH$_2$−), 1.86 (m, 9H, −CH$_2$−), 4.07 (m, 6H, −OCH$_2$−), 6.97 (s, 2H, −C≡CC_6H_2−), 7.53 (m, 4H, naphthyl of C^N^C), 7.81 (d, 2H, J = 7.8 Hz, pyridine of C^N^C), 7.90 (m, 3H, naphthyl and pyridine of C^N^C), 8.01 (m, 4H, naphthyl of C^N^C), 8.37 (m, 2H, naphthyl of C^N^C). Positive FAB-MS: m/z 1433 ([M]$^+$). IR (KBr): 2152 cm^{-1} [ν(C≡C)]. Elem anal. Calcd for $C_{87}H_{128}AuNO_3$ (found): C, 72.92 (73.16); H, 9.00 (9.04); N, 0.98 (1.39).

■ ASSOCIATED CONTENT

Ⓢ Supporting Information

Crystallographic data for the structures of **1** and **5**, temperature-dependent UV−vis absorption spectral traces, and emission spectra of the sol−gel phase transition of complex **4** in cyclohexane. This material is available free of charge via the Internet at http://pubs.acs.org.

■ AUTHOR INFORMATION

Corresponding Author

*E-mail: wwyam@hku.hk.

Notes

The authors declare no competing financial interest.

■ ACKNOWLEDGMENTS

V.W.-W.Y. acknowledges support from The University of Hong Kong and the URC Strategic Research Theme on Molecular Materials. This work has been supported by the University Grants Committee Areas of Excellence Scheme (AoE/P-03/08), the Collaborative Research Fund (HKUST2/CRF/10), and the General Research Fund (HKU 7060/09P and HKU 7063/10P) from the Research Grants Council of Hong Kong Special Administrative Region, People's Republic of China. V.K.-M.A. acknowledges the receipt of a postgraduate studentship from The University of Hong Kong. Dr. A. Y.-Y. Tam is gratefully acknowledged for his helpful discussions on gelation studies. Dr. L. Szeto is gratefully acknowledged for technical assistance in the crystal structure determination of **1**. We also thank the Electron Microscope Unit at The University of Hong Kong for their technical assistance.

■ DEDICATION

Dedicated to Professor Dieter Fenske on the occasion of his 70th birthday.

■ REFERENCES

(1) Pyykkö, P. *Chem. Rev.* **1988**, *88*, 563.

(2) (a) Ford, P. C.; Vogler, A. *Acc. Chem. Res.* **1993**, *26*, 220. (b) Vogler, A.; Kunkely, H. *Coord. Chem. Rev.* **2001**, *219−221*, 489.

(3) (a) Schmidbaur, H. *Chem. Soc. Rev.* **1995**, *24*, 391. (b) Hutchings, G. J.; Brust, M.; Schmidbaur, H. *Chem. Soc. Rev.* **2008**, *37*, 1759.

(4) Schmidbaur, H., Ed. *Gold: Progress in Chemistry, Biochemistry and Technology*; John Wiley & Sons: Chichester, U.K., 1999.

(5) Fung, E. Y.; Olmstead, M. M.; Vickery, J. C.; Balch, A. L. *Coord. Chem. Rev.* **1998**, *171*, 151.
(6) Burini, A.; Mohamed, A. A.; Fackler, J. P., Jr. *Comments Inorg. Chem.* **2003**, *24*, 253.
(7) Laguna, A., Ed. *Modern Supramolecular Gold Chemistry*; Wiley-VCH: Weinheim, Germany, 2008.
(8) Mohr, F., Ed. *Gold Chemistry: Applications and Future Directions in the Life Sciences*; Wiley-VCH: Weinheim, Germany, 2009.
(9) Corti, C., Holliday, R., Eds. *Gold: Science and Applications*; CRC Press: Boca Raton, FL, 2010.
(10) Puddephatt, R. J. *Chem. Soc. Rev.* **2008**, *37*, 2012.
(11) (a) Yam, V. W.-W.; Lo, K. K.-W. *Chem. Soc. Rev.* **1999**, 323. (b) Yam, V. W.-W.; Cheng, E. C.-C. *Top. Curr. Chem.* **2007**, *281*, 269. (c) Yam, V. W.-W.; Cheng, E. C.-C. *Chem. Soc. Rev.* **2008**, *37*, 1806. (d) He, X.; Yam, V. W.-W. *Coord. Chem. Rev.* **2011**, *255*, 2111.
(12) Terech, P.; Weiss, R. G. *Chem. Rev.* **1997**, *97*, 3133.
(13) Sangeetha, N. M.; Maitra, U. *Chem. Soc. Rev.* **2005**, *34*, 821.
(14) Weiss, R. G., Terech, P., Eds. *Molecular Gels. Materials with Self-Assembled Fibrillar Networks*; Springer: Dordrecht, The Netherlands, 2005.
(15) Llusar, M.; Sanchez, C. *Chem. Mater.* **2008**, *20*, 782.
(16) Steed, J. W. *Chem. Commun.* **2011**, *47*, 1379.
(17) Ajayaghosh, A.; Praveen, V. K.; Vijayakumar, C. *Chem. Soc. Rev.* **2008**, *37*, 109.
(18) Dastidar, P. *Chem. Soc. Rev.* **2008**, *37*, 2699.
(19) (a) Xia, Y.; Yang, P. *Adv. Mater.* **2003**, *15*, 351. (b) Xia, Y.; Yang, P.; Sun, Y.; Wu, Y.; Mayers, B. T.; Gates, B.; Yinn, Y.; Kim, F.; Yan, H. *Adv. Mater.* **2003**, *15*, 353.
(20) Piepenbrock, M.-O. M.; Lloyd, G. O.; Clarke, N.; Steed, J. W. *Chem. Rev.* **2010**, *110*, 1960.
(21) Fages, F. *Angew. Chem., Int. Ed.* **2006**, *45*, 1680.
(22) Stang, P. J.; Olenyuk, B. *Acc. Chem. Res.* **1997**, *30*, 502.
(23) (a) Fujita, M. *Chem. Soc. Rev.* **1998**, *27*, 417. (b) Fujita, M.; Ogura, K. *Coord. Chem. Rev.* **1996**, *148*, 249.
(24) Sun, S.-S.; Lees, A. J. *Coord. Chem. Rev.* **2002**, *230*, 171.
(25) (a) Yam, V. W.-W.; Wong, K. M.-C.; Hung, L.-L.; Zhu, N. *Angew. Chem.* **2005**, *117*, 3167. (b) Wong, K. M. C.; Zhu, X.; Hung, L.-L.; Zhu, N.; Yam, V. W.-W.; Kwok, H.-S. *Chem. Commun.* **2005**, 2906. (c) Wong, K. M.-C.; Hung, L.-L.; Lam, W. H.; Zhu, N.; Yam, V. W.-W. *J. Am. Chem. Soc.* **2007**, *129*, 4350. (d) Au, V. K.-M.; Wong, K. M.-C.; Zhu, N.; Yam, V. W.-W. *J. Am. Chem. Soc.* **2009**, *131*, 9076. (e) Au, V. K.-M.; Wong, K. M.-C.; Tsang, D. P.-K.; Chan, M.-Y.; Zhu, N.; Yam, V. W.-W. *J. Am. Chem. Soc.* **2010**, *132*, 14273.
(26) Yam, V. W.-W.; Choi, S. W.-K.; Lai, T.-F.; Lee, W.-K. *J. Chem. Soc., Dalton Trans.* **1993**, 1001.
(27) Au, V. K.-M.; Wong, K. M.-C.; Zhu, N.; Yam, V. W.-W. *Chem.—Eur. J.* **2011**, *17*, 130.
(28) (a) Garg, J. A.; Blacque, O.; Fox, T.; Venkatesan, K. *Inorg. Chem.* **2010**, *49*, 11463. (b) Garg, J. A.; Blacque, O.; Venkatesan, K. *Inorg. Chem.* **2011**, *50*, 5430.
(29) Bojan, V. R.; López-de-Luzuriaga, J. M.; Manso, E.; Monge, M.; Olmos, M. E. *Organometallics* **2011**, *30*, 4486.
(30) (a) Hirst, A. R.; Smith, D. K.; Feiters, M. C.; Geurts, H. P. M. *Langmuir* **2004**, *20*, 7070. (b) Hirst, A. R.; Smith, D. K.; Feiters, M. C.; Geurts, H. P. M. *Chem.—Eur. J.* **2004**, *10*, 5901.
(31) Vemula, P. K.; John, G. *Chem. Commun.* **2006**, 2218.
(32) Smith, D. K. In *Organic Nanostructures*; Atwood, J. L., Steed, J. W., Eds.; Wiley-WCH: Weinheim, Germany, 2008; p 111.
(33) Maeda, H. *Chem.—Eur. J.* **2008**, *14*, 11274.
(34) Peng, F.; Li, G.; Liu, X.; Wu, S.; Tong, Z. *J. Am. Chem. Soc.* **2008**, *130*, 16166.
(35) Wang, S.; Shen, W.; Feng, Y.; Tian, H. *Chem. Commun.* **2006**, 1497.
(36) Kamikawa, Y.; Kato, T. *Langmuir* **2007**, *23*, 274.
(37) (a) Tam, A. Y.-Y.; Wong, K. M.-C.; Wang, G.-X.; Yam, V. W.-W. *Chem. Commun.* **2007**, 2028. (b) Tam, A. Y.-Y.; Wong, K. M.-C.; Yam, V. W.-W. *Chem.—Eur. J.* **2009**, *15*, 4775. (c) Tam, A. Y.-Y.; Wong, K. M.-C.; Yam, V. W.-W. *J. Am. Chem. Soc.* **2009**, *131*, 6253. (d) Tam, A. Y.-Y.; Wong, K. M.-C.; Zhu, N.; Wang, G.-X.; Yam., V. W.-W. *Langmuir* **2009**, *25*, 8685. (e) Li, Y.; Tam, A. Y.-Y.; Wong, K. M.-C.; Li, W.; Wu, L.; Yam, V. W.-W. *Chem.—Eur. J.* **2011**, *17*, 8048. (f) Cameral, F.; Ziessel, R.; Donnio, B.; Bourgogne, C.; Guillon, D.; Schmutz, M.; Iacovita, C.; Bucher, J. P. *Angew. Chem., Int. Ed.* **2007**, *46*, 2659. (g) Shirakawa, M.; Fujita, N.; Tani, T.; Kaneko, K.; Shinkai, S. *Chem. Commun.* **2005**, 4149.
(38) (a) Lu, W.; Law, Y.-C.; Han, J.; Chui, S. S.-Y.; Ma, D.-L.; Zhu, N.; Che, C.-M. *Chem.—Asian J.* **2008**, *3*, 59. (b) Wang, J.; Chen, Y.; Law, Y.-C.; Li, M.; Zhu, M.-X.; Lu, W.; Chui, S. S.-Y.; Zhu, N.; Che, C.-M. *Chem.—Asian J.* **2011**, *6*, 3011.
(39) (a) Zhang, J.; Xu, X.-D.; Chen, L.-J.; Luo, Q.; Wu, N.-W.; Wang, D.-X.; Zhao, X.-L.; Yang, H.-B. *Organometallics* **2011**, *30*, 4032. (b) Xu, X.-D.; Zhang, J.; Chen, L.-J.; Zhao, X.-L.; Wang, D.-X.; Yang, H.-B. *Chem.—Eur. J.* **2012**, *18*, 1659.
(40) Cardolaccia, T.; Li, Y.; Schanze, K. S. *J. Am. Chem. Soc.* **2008**, *130*, 2535.
(41) Kishimura, A.; Yamashita, T.; Aida, T. *J. Am. Chem. Soc.* **2005**, *127*, 179.
(42) He, Y.; Bian, Z.; Kang, C.; Cheng, Y.; Guo, L. *Chem. Commun.* **2010**, *46*, 3532.
(43) Kawano, S.; Fujita, N.; Shinkai, S. *J. Am. Chem. Soc.* **2004**, *126*, 8592.
(44) (a) Lam, S.-T.; Wang, G.-X.; Yam, V. W.-W. *Organometallics* **2008**, *27*, 4545. (b) Lam, S.-T.; Yam, V. W.-W. *Chem.—Eur. J.* **2010**, *16*, 11588.
(45) Fujigaya, T.; Jiang, D.-L.; Aida, T. *Chem.—Asian J.* **2007**, *2*, 106.
(46) Wong, K.-H.; Cheung, K.-K.; Chan, M. C.-W.; Che, C.-M. *Organometallics* **1998**, *17*, 3505.
(47) (a) Provot, O.; Giraud, A.; Peyrat, J. F.; Alami, M.; Brion, J. D. *Tetrahedron Lett.* **2005**, *46*, 8547. (b) Wu, J.; Watson, M. D.; Zhang, L.; Wang, Z.; Müllen, K. *J. Am. Chem. Soc.* **2004**, *126*, 177.
(48) Kröhnke, F. *Synthesis* **1976**, 1.
(49) (a) Demas, J. N.; Crosby, G. A. *J. Phys. Chem.* **1971**, *75*, 991. (b) Van Houten, J.; Watts, R. *J. Am. Chem. Soc.* **1976**, *98*, 4853.
(50) Connelly, N. G.; Geiger, W. E. *Chem. Rev.* **1996**, *96*, 877.
(51) *SHELXS 97*: Sheldrick, G. M. *SHELXS 97: Programs for Crystal Structure Analysis*, release 97-2; University of Göttingen: Göttingen, Germany, 1997.